ETS-10 as a photocatalyst

Yuni K. Krisnandi,[1] Peter D. Southon,[1] Asoji A. Adesina,[2] and Russell F. Howe[1,†]

[1] *Chemistry Department, University of Aberdeen, AB24 3UE, Scotland*

[2] *School of Chemical Engineering, UNSW, Sydney, NSW 2052, Australia*

ABSTRACT. ETS-10 is a microporous titanosilicate zeolite with a framework containing linear Ti – O – Ti – O– chains. This paper describes an investigation of the photoreactivity of ETS-10 with the particular objective of evaluating the potential of this novel material as a zeolitic photocatalyst. The photoreactivity and photocatalytic activity of ETS-10 are strongly influenced by defects in the structure. A relatively defect free material catalyses photo-polymerisation of ethene, and in the presence of oxygen catalyses the partial oxidation of ethene to acetic acid and acetaldehyde, which remain strongly adsorbed in the pores. A more defective material is photoreduced when irradiated in the presence of adsorbed ethene, and catalyses the complete oxidation of ethene to carbon dioxide and water in the presence of oxygen. These differences are attributed to differences in the concentrations of exposed titanium sites associated with defects in the ETS-10 structure.

1. INTRODUCTION

ETS-10 is a microporous titanosilicate with a three dimensional 12-ring pore structure, as shown in Figure 1. It contains columns of TiO_6 octahedra linked to silica tetrahedra, with a stoichiometry $(Na,K)_2TiSi_5O_{13}$ [1, 2]. The structure is intrinsically disordered, comprising random intergrowths of two different polymorphs. The TiO_6 chains have been described as one dimensional semiconducting wires within an insulating silica sheath, and band structure calculations for the TiO_6 chains have been reported [3, 4]. The apparent band gap of ETS-10 is blue shifted relative to that of anatase by an amount consistent with quantum confinement in a one-dimensional nanosemiconductor.

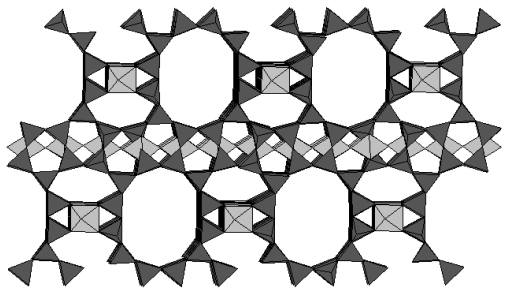

Figure 1. *Structure of ETS-10.* TiO_6 *octahedra are shaded light grey, and* SiO_4 *tetrahedra are shaded dark grey.*

Anatase is well known as a photocatalyst for oxidation of organic molecules in the gas phase [5]. The photocatalytic efficiency of anatase and other particulate semiconducting oxides is limited by the competition between hole:electron recombination, and the reactions of holes and electrons with adsorbed species at the particle surfaces. The apparent semiconducting properties of ETS-10, and the high surface area available within the open micropores of the structure, prompted us to investigate its potential as a photocatalyst for simple gas phase reactions. The ability to place reactant molecules in close proximity to the semiconductor chains in ETS-10 may in principle allow more efficient interception of photo-produced holes and electrons by the adsorbed species than is possible with a conventional particulate semiconductor. Two preliminary studies of ETS-10 as a photocatalyst have been reported [6, 7]. This paper describes an investigation of the photoreactivity of ETS-10 towards ethene, and a comparison of its photocatalytic activity for the oxidation of gaseous ethene with that of a conventional anatase photocatalyst. A preliminary communication from this work was recently published [8].

†E-mail: r.howe@abdn.ac.uk

2. EXPERIMENTAL

2.1. Catalysts. A commercial sample of ETS-10 was provided by Engelhard (Lot FN94015, Code N6070C); this was stated to be in the proton exchanged form. Analysis by X-ray fluorescence gave the unit cell composition $H_{1.55}Na_{0.15}K_{0.30}Si_{4.78}TiO_{13}.\ 4.78H_2O$. Synthetic ETS-10 was prepared following the procedure of Anderson, *et al.* [1], with some modification [9]. Briefly, a gel with oxide composition $3.7\,Na_2O : 0.95\,K_2O : TiO_2 : 5.7\,SiO_2 : 171\,H_2O$ was prepared by mixing sodium silicate solution, $TiCl_3$ (15% solution in HCl) and solid potassium fluoride. A small quantity of commercial ETS-10 was added as a seed, and the gel autoclaved in a Teflon-lined stainless steel autoclave under autogeneous pressure for 10 days at 443 K. The resulting product was filtered, washed and dried. X-ray fluorescence analysis gave the unit cell composition

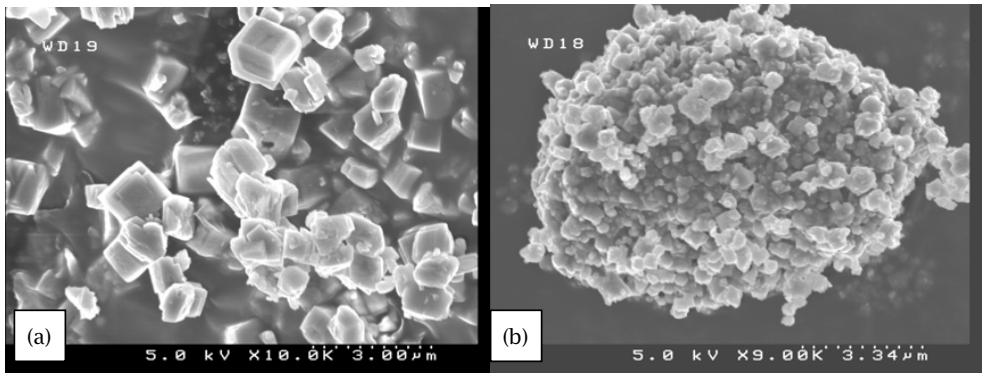

Figure 2. *SEM images of (a) synthetic ETS-10 and (b) commercial ETS-10.*

$Na_{1.60}K_{0.44}Si_{4.96}TiO_{13}$. $3.44H_2O$. For comparison purposes, a commercial anatase sample (Degussa P25, 79% anatase, 21% rutile, $50\,m^2g^{-1}$) was employed.

2.2. Catalyst characterisation. ETS-10 samples were characterised by X-ray powder diffraction (Siemens D500, Cu Kα radiation), scanning electron microscopy (Hitachi 4500 FESEM), Raman spectroscopy (Renishaw 2000 Raman Microprobe, 514 nm excitation), UV-VIS spectroscopy (Cary 5 fitted with diffuse reflectance accessory) and ^{29}Si MASNMR spectroscopy (Varian Innova 300, 2.5 kHz MAS, 2 microsecond pulse-width with high power proton decoupling and 60 second pulse delay). Surface area measurements were performed on a Micromeritics Accusorb 2000 instrument. Ti K-edge XANES and EXAFS measurements were undertaken at the Australian National Beamline Facility, the Photon Factory, Japan. Data were collected in transmission mode at 15 K using a closed cycle cryostat. Data analysis utilised the XFIT and FEFFIT software package [10–12].

2.3. In-situ spectroscopic measurements. FTIR measurements used a pyrex and quartz high vacuum cell in which pressed disks of catalyst could be outgassed, exposed to reactant gases and irradiated in-situ. Spectra were recorded on a Bomem MB100 FTIR spectrometer equipped with an MCT detector, at $4\,cm^{-1}$ resolution. EPR measurements employed a pyrex high vacuum cell fitted with a quartz side-arm which likewise allowed outgassing and irradiation of samples prior to measuring spectra at 77 K in a liquid nitrogen insert dewar. EPR spectra were recorded at X-band on a Bruker EMX spectrometer. For both FTIR and EPR experiments, the UV irradiation source was a 125 W medium pressure mercury lamp.

2.4. Photocatalytic measurements. A fluidised bed reactor was used to evaluate catalyst performance. Catalyst (typically 0.5 g) was pelletised to a 50 μm particle size and held between quartz wool plugs in a 180 mm $\times$ 8 mm o.d. quartz tube. Fluidisation was achieved by passing a nitrogen flow through the bed, to which ethylene and oxygen were added as desired, using mass flow controllers. Catalyst samples were initially outgassed by heating in flowing nitrogen to 423 K for 2 hours. The furnace was then removed and the reactor was surrounded with an aluminum reflector directing light from a medium pressure mercury arc lamp onto the reactor from all sides. In most experiments, compressed air was directed onto the reactor to minimise heating during irradiation. Effluent gases from the reactor were analysed on-line with a Shimadzu GC8A gas chromatograph fitted with a Carbosphere column and a TCD detector, coupled to a Shimadzu CR3A integrator.

3. RESULTS AND DISCUSSION

3.1. Catalyst characterisation. X-ray powder diffraction patterns (not shown) of the commercial and synthesised ETS-10 samples show the peaks expected for the ETS-10 structure [1]. Those for the synthetic sample are generally more intense than for the commercial sample, and particularly at higher angles the diffraction peaks for the commercial sample are severely broadened. Yang and Blosser [13] have suggested that such broadening is due to the higher concentrations of stacking faults and other defects in the commercial sample. This suggestion is supported by very clear differences in crystal size and morphology between the two samples revealed in SEM images shown in Figure 2. In particular, the commercial sample shows considerably smaller crystallite size and much less regular morphology than the synthesised sample.

Recent work in our laboratory has shown that repeated ion exchange procedures with a well crystalline synthetic ETS-10 degrade the crystal morphology, resulting in SEM images not unlike those of the commercial sample shown in Figure 2 [14]. Although the prior history of the commercial ETS-10 sample is not known, it will have been produced from an as-synthesised sample either by direct proton exchange or indirectly

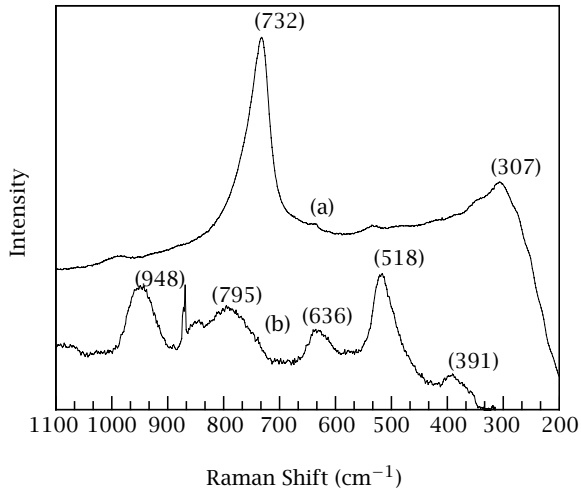

Figure 3. *Raman spectra of (a) synthetic ETS-10, (b) commercial ETS-10.*

through ammonium ion exchange and calcination [15]. In either case, this treatment will increase the concentrations of defects in the structure.

The Raman spectrum of ETS-10 is particularly sensitive to the presence of stacking faults in the structure. As shown in Figure 3, a well crystalline sample of ETS-10 gives an intense Raman band at around 730 cm^{-1} which has been assigned to Ti–O–Ti stretching modes in the O–Ti–O–Ti–O chains [16]. In work published elsewhere [17] we have shown that the intensity, frequency and half-width of this band are critically dependent on the long range order in the structure. In ETS-10 preparations with higher concentrations of stacking faults, the average O–Ti–O–Ti–O chain length is shortened, which perturbs the Raman active stretching mode without necessarily altering the powder diffraction pattern. In commercial ETS-10 the 732 cm^{-1} band is broadened, reduced in intensity and shifted to about 800 cm^{-1}. The reduction in intensity of this band in the commercial sample allows weaker bands in the spectrum to be more clearly seen. We conclude from the Raman spectra that the commercial ETS-10 sample is much more defective than the synthetic sample.

Further support for this conclusion comes from the results of Ti K-edge EXAFS measurements, which will be reported in detail elsewhere [18]. The EXAFS is sensitive to variations in the short range order around the titanium sites in ETS-10. Sankar, *et al.* [19] have shown that the Ti K-edge EXAFS from a well-crystalline ETS-10 can be fitted to a structural model including alternating short and long Ti–O bonds along the O–Ti–O–Ti–O chains. The corresponding data for the commercial ETS-10 sample differ in two respects: the first coordination shell is modified (the peak in the Fourier transform is less tense), and the peaks at longer distances have become much less distinct. Both of these differences are indicative of a more heterogeneous and defective environment for the titanium in the commercial sample.

Comparison of ^{29}Si NMR spectra of the two samples (not shown) also indicates that the commercial sample is less well ordered than the synthetic sample. The three major peaks in the spectrum of synthetic ETS-10 at −94, −96.3 and −103.4 ppm (relative to TMS) are broadened and shifted to higher field in the commercial sample (−97.5, −100 and −110 ppm). Yang and Truitt [20] attributed these differences previously to replacement of Na and K cations by protons, although our work shows that structural differences must also be contributing [17].

To summarise the above discussion, the two ETS-10 samples used in this work, although both having the stoichiometry and X-ray powder diffraction pattern of ETS-10, differ substantially in the levels of defects present in the structure. This difference may be expected to influence the photoreactivity in two ways. Interruption of the O–Ti–O–Ti–O chains through stacking faults or other defects will alter the effective length of the chains and therefore affect the band gap of the semiconductor. Secondly, defects introduced into the structure will provide localised states within the band gap, and may also provide specific surface sites for adsorption or reaction to occur. A further difference between the synthetic and commercial ETS-10 samples used in this work is the cation exchange level, which may also influence reactivity.

3.2. In-situ EPR studies. A well known feature of the photoreactivity of anatase is photoreduction when the catalyst is irradiated in the presence of adsorbed organic molecules. The explanation proposed for this observation is that the adsorbed organic molecules function as scavengers of photo-produced holes, leaving electrons to be trapped at Ti^{4+} sites [21]. Figure 4 shows EPR spectra recorded at 77 K following irradiation of an anatase sample at room temperature in the presence of ethene. An intense signal with an axial g-tensor ($g_\perp = 1.973$, $g_\parallel = 1.949$) appeared and grew in intensity with irradiation time. This signal is closely similar to that of the Ti^{3+} obtained when anatase is heated in the presence of ethene ($g_\perp = 1.972$, $g_\parallel = 1.948$ [21]). Admission of a small pressure of oxygen (8 torr) had no effect on the Ti^{3+} signal, but exposure to oxygen after evacuation of ethene caused complete removal of the Ti^{3+} signal. It is noteworthy that no superoxide (O_2^-) signals were obtained on admission of oxygen, implying that the reduced titanium species are present in the anatase bulk and not present as surface sites. The Ti^{3+} signal could not be detected at room temperature, suggesting that this species is present in a relatively undistorted coordination, having efficient spin-lattice relaxation.

The same experiment performed with synthetic ETS-10 gave no EPR signals at room temperature or 77K,

Table 1. *g-tensor components of* Ti^{3+} *species.*

sample	treatment	$g_\perp$	$g_\parallel$	reference
anatase	Thermal reduction in ethene	1.972	1.948	[22]
anatase	Photoreduction in ethene	1.973	1.949	This work
ETS-10(comm)	Photoreduction in ethene	1.954	1.927	This work
ETS-10	Reduced in H_2 at 673 K	1.941	1.966	[23]
ETS-10	Reduced in NaN_3	1.935	1.857	[4]
		1.915	1.860	

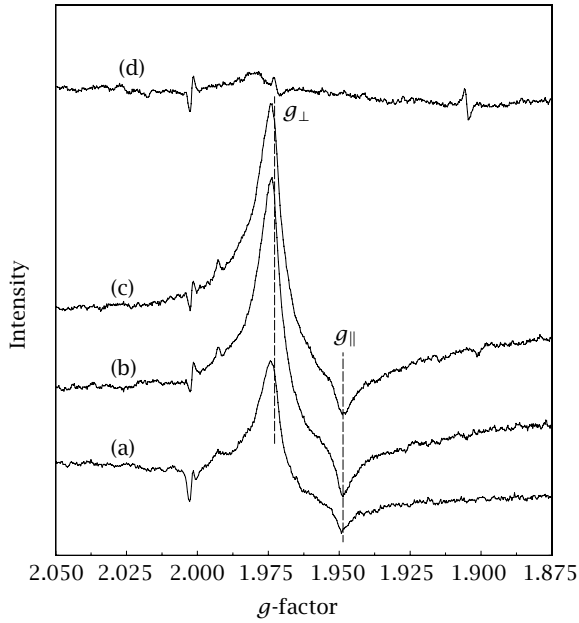

Figure 4. *EPR spectra of anatase at 77K after UV irradiation in ethene for (a) 30 minutes, (b) 60 minutes, (c) after addition of 8 torr of oxygen, (d) evacuated and exposed to 8 torr of oxygen.*

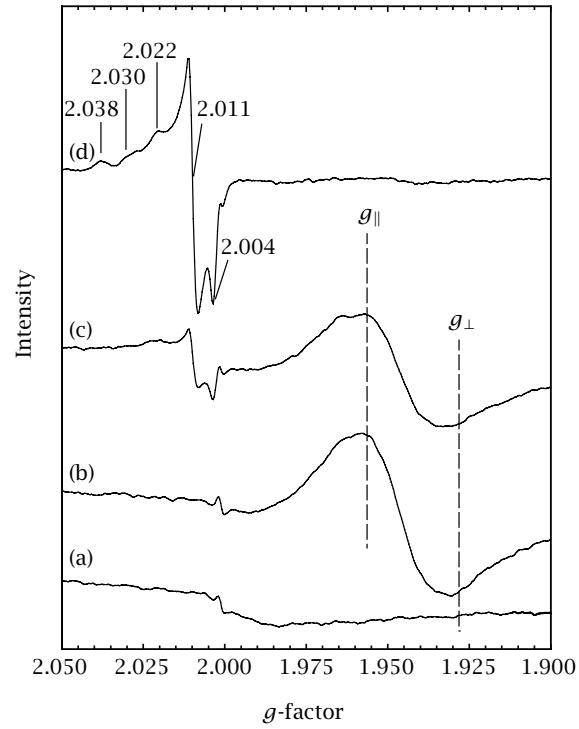

Figure 5. *EPR spectra of commercial ETS-10 at room temperature (a) exposed to ethene, (b) irradiated 2 hours, (c) exposed to 5 torr of oxygen, (d) evacuated and exposed to 5 torr of oxygen.*

i.e. the titanium in synthetic ETS-10 was not reduced when irradiated in the presence of adsorbed ethene. Photoreduction was observed however when the commercial sample was irradiated under the same conditions. Figure 5 shows spectra recorded at room temperature following irradiation of a sample of commercial ETS-10 in the presence of 50 torr of ethene at room temperature. An intense broad signal with g-tensor components $g_\perp = 1.954$ and $g_\parallel = 1.927$ appeared and increased in intensity with increasing irradiation time.

Table 1 compares the g-tensor components of the signals observed here with those of Ti^{3+} in other systems. The signal from photoreduced commercial ETS-10 differs from that obtained with anatase in two respects: the g-tensor components are different, and the spin lattice relaxation time is longer, allowing signals to be measured at room temperature. The Ti^{3+} formed on photoreduction differs also from those obtained by thermal reduction of ETS-10 in hydrogen at 673 K [23] and on treatment of the sodium form of ETS-10 with sodium azide at 600 K [4]. All of these signals have g-tensor components broadly consistent with Ti^{3+} cations in distorted octahedral coordination; however, the extent of distortion will influence significantly the g-tensors obtained. The low temperature conditions of photoreduction might be expected to preserve the site geometry of the Ti^{4+} species being reduced more strictly than the higher temperature treatments.

The photoreduced Ti^{3+} species in commercial ETS-10 also differ from those in anatase in their reactivity towards oxygen. Evacuation of ethene and admission of a low pressure of oxygen gives a strong signal characteristic of the superoxide ion, and causes removal of the Ti^{3+} signal. Closer examination of the superoxide signal reveals that at least three different species are present, with different values of the low field (g_{11}) g-tensor component. The g_{11} component of the superoxide ion adsorbed on surfaces is known to be sensitive to the electrostatic charge on the cation site on which it is adsorbed, whereas the g_{22} and g_{33} components always

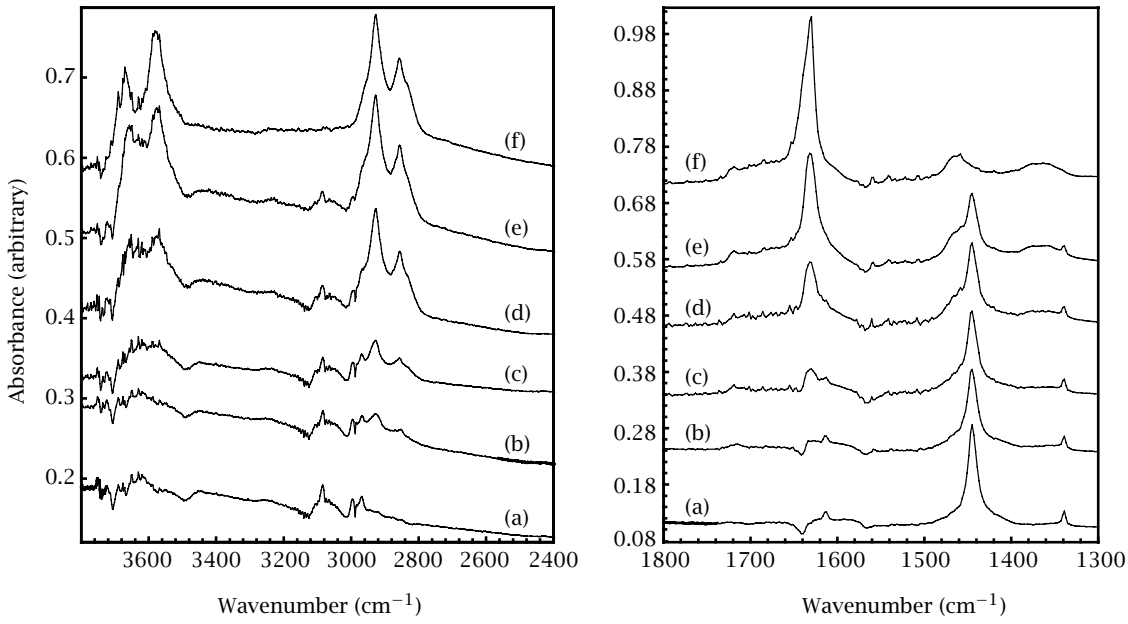

Figure 6. *FTIR difference spectra of ethene in synthetic ETS-10 (a) exposed to 70 torr of ethene, (b) irradiated 60 minutes, (c) 120 minutes, (d) 300 minutes, (e) 510 minutes, (f) evacuated at room temperature.*

have similar values ($g_{22} \approx 2.010$ and $g_{33} \approx 2.003$) [24]. The major g_{11} component on ETS-10 is similar to that seen for superoxide adsorbed on Ti^{4+} sites ($g_{11} \approx 2.022$), whereas the other components at lower field are typical of superoxide adsorbed on sites of lower formal charge. Superoxide adsorbed on thermally reduced ETS-10 gives a very similar signal to that seen here ($g_{11} = 2.021$, $g_{22} = 2.008$, $g_{33} = 2.002$) [23], whereas on sodium azide treated ETS-10 the g_{11} component of adsorbed superoxide is shifted to 2.084 [4]. The additional components in the spectrum obtained from photoreduced commercial ETS-10 (2.038, 2.030) cannot therefore be due to superoxide adsorbed on Na^+ or K^+ sites, but we are unable, at present, to identify these components. Regardless, the ability of photoreduced ETS-10 to generate superoxide ions, particularly superoxide ions adsorbed on Ti^{4+} sites, indicates that titanium sites in commercial ETS-10 are freely accessible to oxygen molecules.

The possibility that the photoreactivity (photoreduction) of ETS-10 may depend solely on the exchanged cations present (i.e. Na^+ and K^+ in synthetic ETS-10 versus predominantly H^+ in commercial ETS-10) has been ruled out by preparing an ammonium exchanged form of the synthetic sample, then back-exchanging this again with sodium cations. When the ammonium exchanged version of synthetic ETS-10 is outgassed in vacuo, ammonia is evolved and the proton-exchanged form of the zeolite is obtained. This HETS-10 sample also showed photoreduction when irradiated in ethene at room temperature. However, photoreduction was also seen when the back-exchanged NaETS-10 was irradiated in ethane, i.e. photoreduction is not dependent on the presence of protons as the exchanged cation in ETS-10. As discussed further below, defects introduced during the ion exchange process are the key element in promoting photoreduction.

3.3. In-situ FTIR experiments. Figure 6 shows infrared difference spectra obtained when synthetic ETS-10 was UV irradiated at room temperature in the presence of 70 torr of ethene. The spectrum of the initial outgassed ETS-10 sample prior to introduction of ethene has been subtracted, and all bands due to gas phase species have also been subtracted. The spectrum obtained on initial exposure to ethene shows bands characteristic of physically adsorbed ethene, at around 3080 cm^{-1} (ν(CH)), 1615 cm^{-1} (ν(C = C)), 1445 and 1340 cm^{-1} ($\delta(CH_2)$). On irradiation, these bands were gradually diminished in intensity. At the same time, new bands appeared at 3654, 3570, 2926, 2856, 1632, 1468 and 1364 cm^{-1}. These new bands grew in intensity with irradiation time over several hours. Subsequent evacuation at room temperature removed the bands due to residual physically adsorbed ethene, but the new bands formed by irradiation were unchanged.

Blank experiments established that the changes described were observed only under UV irradiation. Prolonged exposure to ethene at room temperature in the dark caused no changes in the infrared spectrum.

The new bands appearing at 2926, 2856, 1468 and 1364 cm^{-1} are assigned to a saturated polyethene

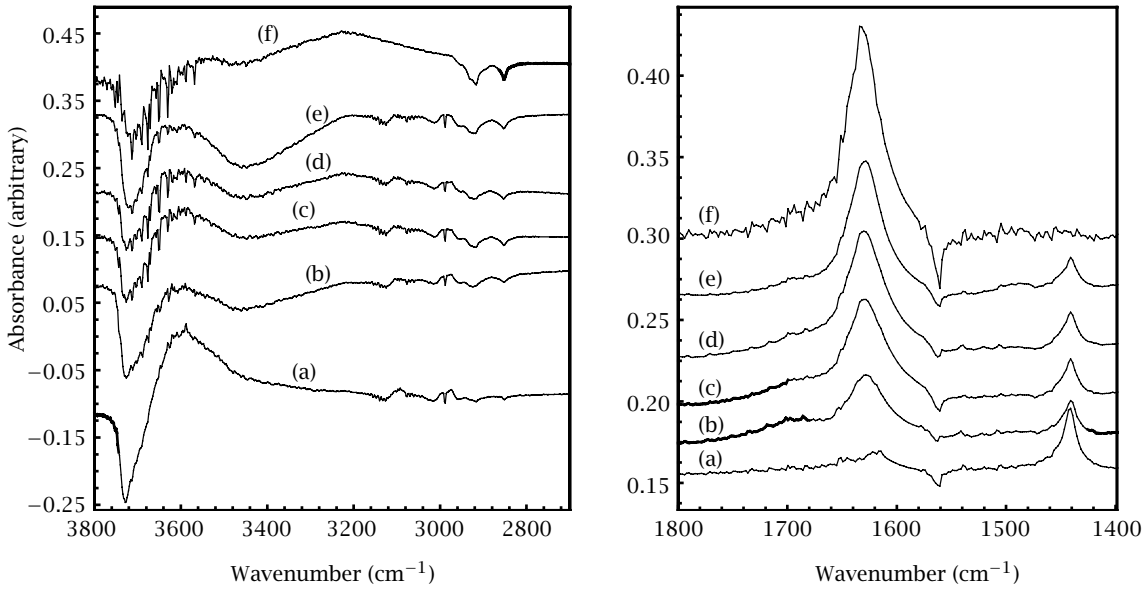

Figure 7. *FTIR difference spectra of ethene in commercial ETS-10 (a) exposed to 50 torr of ethene, (b) irradiated 60 minutes, (c) 90 minutes, (d) 120 minutes, (e) 180 minutes, (f) evacuated at room temperature.*

$(CH_2)_n$ species. Such polyethene chains are expected to show symmetric and asymmetric $\nu(CH_2)$ and $\delta(CH_2)$ vibrational modes in these regions [25]. The new bands at 3654, 3570 and 1632 cm^{-1}, on the other hand, are close to the frequencies expected for isolated water molecules (ν(OH) and δ(HOH) modes, respectively) [26]. Water adsorbed in zeolites is usually in hydrogen bonded liquid form, giving rise to a broad composite ν(OH) band at around 3400 cm^{-1} and a δ(HOH) band at around 1620 cm^{-1}. We have, however, also observed the narrow well-resolved bands described above in non-irradiated synthetic ETS-10 following evacuation at room temperature, indicating that in this particular zeolite isolated water molecules can be adsorbed within the pores.

Figure 7 shows FTIR difference spectra obtained during the same experiment carried out with commercial ETS-10. The commercial ETS-10 after outgassing in *vacuo* at 393 K gives a broad intense band in the ν(OH) region at around 3600 cm^{-1} (not shown). This spectrum has been subtracted from all of the spectra in Figure 7, as have the bands due to gas phase species. The intense negative peak at 3735 cm^{-1} in the difference spectrum following admission of ethene, and the appearance of a new positive peak at around 3620 cm^{-1} shows that ethene is weakly hydrogen bonded with those hydroxyl groups in the commercial ETS-10 which are responsible for a band at 3735 cm^{-1}. This band has been previously assigned to SiOH groups in HETS-10 [27]. The spectrum otherwise shows bands of adsorbed ethene similar to those seen in the synthetic ETS-10 sample. On irradiation, the bands due to adsorbed ethene are reduced in intensity, and new bands appear at 1630 cm^{-1} and (very broad) around 3300 cm^{-1}. Evacuation removes the remaining physically adsorbed ethene bands. There is no evidence in this spectrum of any of the bands that were attributed to polyethene in the synthetic ETS-10 sample.

The common feature in these experiments between synthetic and commercial ETS-10 is the formation of water when the ETS-10 is irradiated in the presence of adsorbed ethene. In synthetic ETS-10 these water molecules are isolated within the pores, whereas in commercial ETS-10 the availability of hydroxyl groups for hydrogen bonding means that the adsorbed water molecules give a different spectroscopic signature. The key difference between the two samples of ETS-10 is the formation of polyethene in synthetic ETS-10 without photoreduction of titanium, to be contrasted with the photoreduction occurring in commercial ETS-10.

Formation of water can be attributed to hole scavenging by adsorbed ethene molecules in both zeolites. Hole trapping by oxide ions at the surface of the ETS-10 pores will generate an O^- radical anion. This may extract a hydrogen atom from adsorbed ethene to form a surface hydroxide and an adsorbed ethylidene species [28]. Further hole trapping by the hydroxide species will generate hydroxyl radicals; in commercial ETS-10 with a high concentration of hydroxyl groups hole trapping at hydroxyl groups may be the initiating event. Hydroxyl radicals will then react with adsorbed ethene to form water. The absence of photopolymerisation of ethene in commercial ETS-10, where the EPR experiments have demonstrated the facile trapping of electrons by Ti^{4+}, strongly suggests that the polymerisation observed in synthetic ETS-10 is initiated by

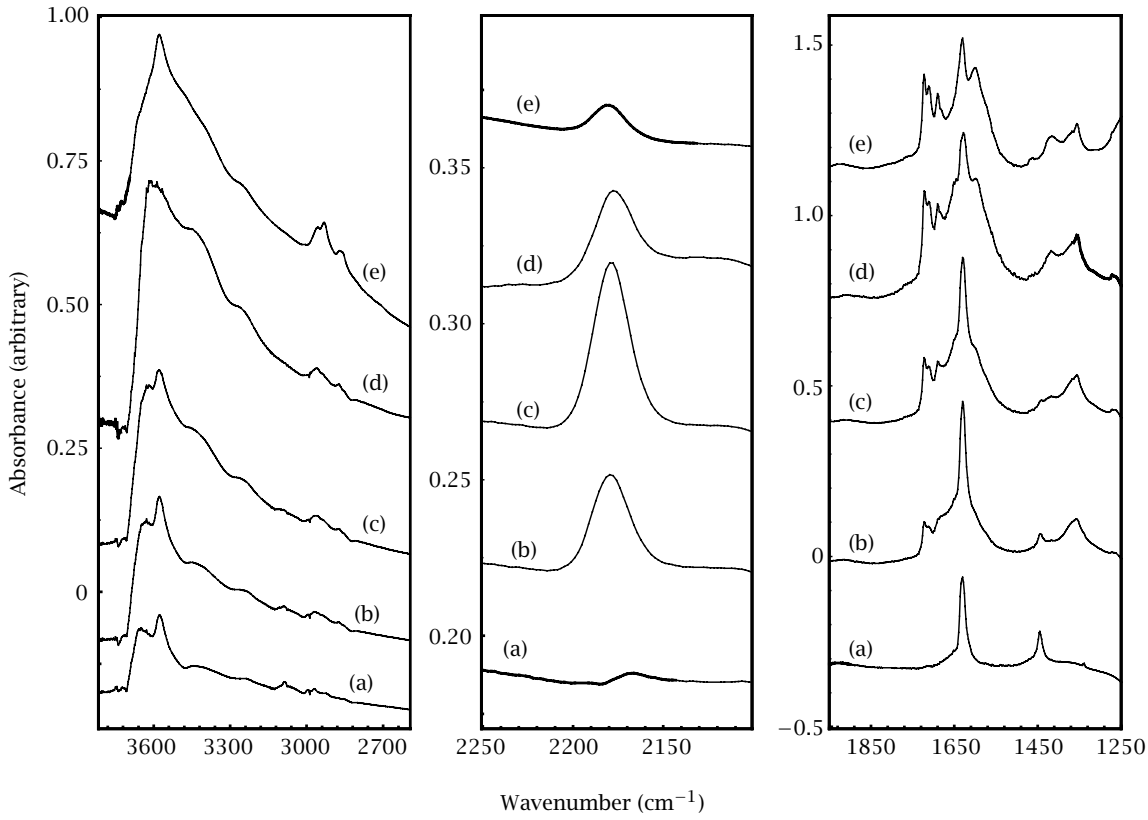

Figure 8. *FTIR difference spectra of synthetic ETS-10 (a) exposed to ethene (40 torr) and oxygen (60 torr), (b) irradiated 60 minutes, (c) 150 minutes, (d) 330 minutes, (e) evacuated at room temperature.*

electron trapping by adsorbed ethene, followed by a free radical polymerisation. This can occur only where Ti^{4+} trap sites are not available.

FTIR experiments were also undertaken of the photo-induced reaction between ethene and oxygen in ETS-10. Figure 8 shows difference spectra measured following irradiation of synthetic ETS-10 in the presence of 40 torr of ethene and 60 torr of oxygen containing traces of water. Before irradiation, the spectrum shows the presence of adsorbed water (3654, 3570, 1630 cm^{-1}) and ethene (3087, 1445 cm^{-1}). On irradiation, the bands of adsorbed ethene are gradually diminished, and a number of new bands appear in the spectrum. There is an increase in intensity in the ν(OH) region, indicating formation of further adsorbed water. New bands appear in the ν(CH) region characteristic of saturated hydrocarbons (2962, 2926, 2872, and 2855 cm^{-1}), at 2175 cm^{-1}, and between 1750 and 1350 cm^{-1}. These new bands increased in intensity with irradiation time. The 2175 cm^{-1} band was partially removed by brief outgassing at room temperature, whereas the remaining new bands remained. The spectra of the gas phase in the cell during irradiation showed only the bands expected for ethene; no new gaseous products were detected.

A band at 2175 cm^{-1} has been previously assigned to a CO : Na^+ adduct formed on adsorption of CO in NaETS-10 [29]. We have attempted to assign the other new bands in the ν(CH) and fingerprint regions by comparing the spectra with those of different model compounds adsorbed in ETS-10. On the basis of those comparisons, we conclude that acetic acid and possibly acetaldehyde are formed by the photo-oxidation of ethene in synthetic ETS-10. Table 2 summarises the frequencies of the main infrared bands used to reach that conclusion. These species are all strongly adsorbed in the pores of ETS-10, since no new species could be detected in the gas phase spectra.

Spectra obtained in the same experiment with commercial ETS-10 are shown in Figure 9. In this case, the formation of large amounts of adsorbed water following irradiation in the presence of ethene and oxygen completely obscured the region of the infrared spectrum above 2800 cm^{-1}. There are three clear differences between the two samples. In commercial ETS-10 a band due to adsorbed carbon dioxide at 2340 cm^{-1} grows on irradiation together with the strong band at 1630 cm^{-1} due to adsorbed water (and carbon dioxide could be detected also in the gas phase spectra).There is no trace of the band due to adsorbed carbon monoxide

Table 2. *Infrared frequencies for molecules adsorbed in ETS-10 (cm^{-1}).*

Acetic acid in ETS-10	Acetaldehyde in ETS-10	Observed in photo-oxidation experiments	Vibrational modes
2936	2975	2961	ν(CH)
2856	2919	2933	
	2875	2872	
	2851		
1758	1721	1724	ν(C=O)
1721		1709	
1693		1688	
1517			
1420	1418	1466	δ(CH)
1386	1384	1416	
1367	1353	1369	
		1356	

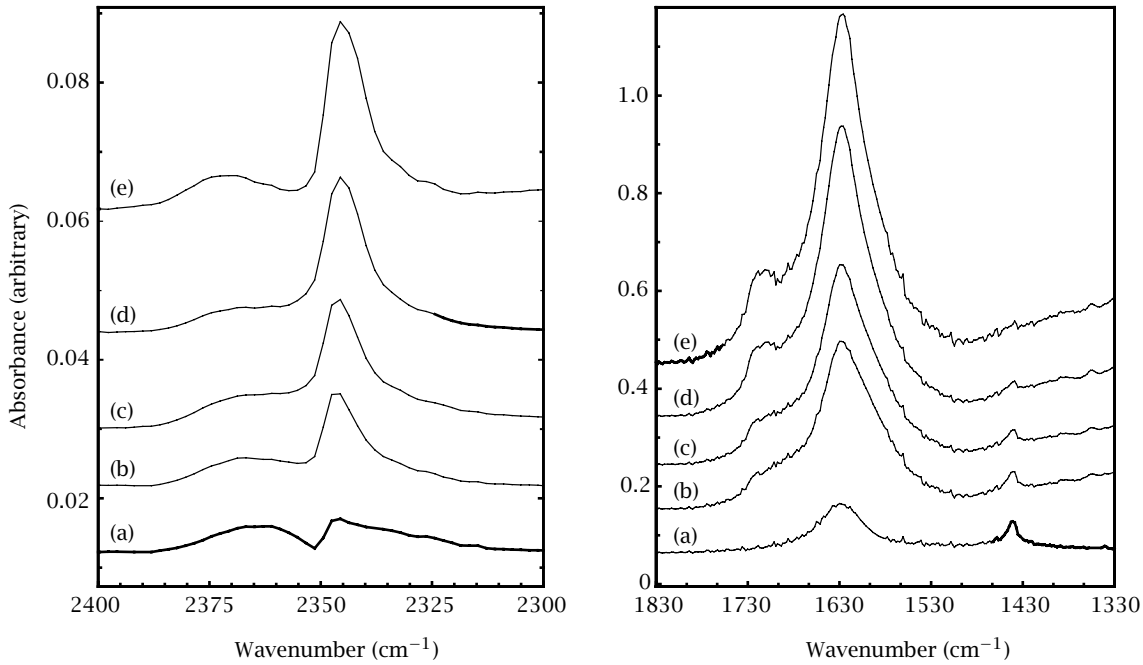

Figure 9. *FTIR difference spectra of commercial ETS-10 (a) exposed to ethene (40 torr) and oxygen (60 torr), (b) irradiated 60 minutes, (c) 90 minutes, (d) 210 minutes, (e) 330 minutes, (f) evacuated at room temperature.*

seen with the synthetic sample. Finally, the contribution to the spectrum from partial oxidation products such as acetic acid (a carbonyl band at 1724 cm^{-1}) is much less than for the synthetic sample.

It appears from these infrared studies that the complete oxidation of ethene to carbon dioxide and water is much more favoured in commercial ETS-10 than in the synthetic sample.

3.4. Photcatalysis studies. Prompted by the different behaviour of the two ETS-10 samples in EPR and FTIR experiments, we undertook continuous flow ethene photo-oxidation experiments in a fluidised bed reactor, comparing ETS-10 with a conventional anatase photocatalyst.

Anatase is well known to photocatalyse the complete oxidation of ethene to carbon dioxide and water [30–32]. Partial oxidation to CO is detected only at low oxygen:ethene ratios [30]. The experiments undertaken here found high conversions of ethene to carbon dioxide over anatase provided the oxygen: ethene ratio was much in excess of stoichiometric, and the temperature was maintained above 473 K (e.g. 70% conversion at an ethene flow rate of 3 mL min^{-1} and an oxygen: ethene ratio of 97 : 1 at 495 K). At lower temperatures the conversion fell, presumably due to poisoning of the catalyst by adsorbed water. The ethene conversion fell to below 10% at all temperatures when the oxygen ethene ratio was decreased to 4 : 1 (at a constant ethene flow rate).

Commercial ETS-10 also showed activity for complete oxidation of ethene to carbon dioxide, although much less than that of anatase. For example, a 7% conversion was achieved under conditions similar to those giving 70% conversions with anatase (3 mL min^{-1}

ethene, oxygen: ethene ratio of 97 : 1 at 573 K), and this fell to ca. 1% at 373 K.

The synthetic ETS-10 catalyst gave no detectable gas phase reaction products under all experimental conditions tried in the flow reactor. Catalysts taken from the reactor nevertheless showed a pronounced yellow colour and an odour of acetic acid.

3.5. Why does commercial ETS-10 behave differently from synthetic ETS-10? The experiments described above have shown that there are many differences between the photoreactivities of anatase, commercial ETS-10 and synthetic ETS-10. In some respects, the commercial ETS-10 resembles anatase in that it does photocatalyse the complete oxidation of ethene to carbon dioxide and water, as demonstrated in both FTIR and catalysis experiments. Nevertheless, the surface chemistry is significantly different. The presence of stacking faults and other defects in ETS-10 will generate exposed titanium sites at the ends of truncated O–Ti–O–Ti–O chains. These sites play a crucial role in the photoreactivity. The titanium sites act as electron traps, allowing photoreduction to occur in the presence of ethene. Electrons trapped at these sites are readily transferred to oxygen, providing a pathway for generating reactive oxygen species. Commercial ETS-10 is a less efficient photocatalyst than anatase on a per gram of catalyst basis, although the activity difference on a per titanium atom basis is much less pronounced. The much higher surface area of ETS-10 compared with P25 anatase may inhibit its catalytic performance for complete oxidation by retaining adsorbed water and carbon dioxide.

Synthetic ETS-10 contains many fewer stacking faults and other defects than the commercial sample, and this has a major influence on its reactivity. In particular, titanium ions in the O–Ti–O–Ti–O chains are not able to act as electron trap sites, but the observed photopolymerisation of ethene in this material appears to involve electron trapping by adsorbed ethene molecules. The observed partial oxidation of ethene to acetic acid within the pores suggests possible future use of such materials for the controlled partial oxidation of reactive molecules. Further study of the reaction pathways in this intra-zeolitic photochemistry are in progress.

Preliminary experiments have indicated that the photoreactivity of the commercial ETS-10 may be reproduced in a synthetic sample by suitable treatment to generate stacking faults (such as ion exchange or thermal treatment).

Finally, this work has demonstrated that the O–Ti–O–Ti–O chains in ETS-10 do indeed demonstrate semiconducting properties. From a photoreactivity perspective, however, it is the defects in the structure which appear to be at least equally important in determining reaction pathways.

ACKNOWLEDGEMENTS

This work was undertaken in part at the University of New South Wales, with support from the Australian Research Council and the Australian Synchrotron Research Program. Y.K. acknowledges support in Australia from AUSAID. Work in Aberdeen is supported by the University of Aberdeen and the Overseas Research Scholarship scheme (Y.K.)

REFERENCES

[1] M. W. Anderson, O. Terasaki, T. Ohsuna, P. J. O. Malley, A. Philippou, S. P. Mackay, A. Ferreire, J.Rocha, and S. Lidin, Phil. Mag. B **71** (1995), 812.
[2] J. Rocha and M. W. Anderson, Eur. J. Inorg. Chem. (2000), 801.
[3] C. Lamberti, Microporous & Mesoporous Mater. **30** (1999), 155.
[4] S. Bordiga, G. T. Palomino, A. Zecchina, G. Ranghino, E. Giamello, and C. Lamberti, J. Chem. Phys. **112** (2000), 3589.
[5] R. F. Howe, Dev. in Chem. Eng. and Mineral Process **6** (1997), 55.
[6] M. A. Fox, K. E. Doan, and M. T. Dulay, Res. Chem. Intermediat **20** (1994), 711.
[7] P. Calza, C. Pazé, E. Pelizzetti, and A. Zecchina, Chem. Comunn. (2001), 2130.
[8] R. F. Howe and Y. K. Krisnandi, Chem. Commun. (2001), 1588.
[9] A. N. Eldewik, Ph.D. Thesis: Spectroscopic Studies of Heavy Metals in Microporous Materials University of New South Wales, Sydney, 1998.
[10] P. A. Ellis and H. C. Freeman, J. Synchrotron Rad. **2** (1995), 190.
[11] A. L. Ankoudinov, Relativistic Spin-dependent X-ray Absorption Theory, Ph.D. Thesis, University of Washington, 1996.
[12] M. Newville, B. Ravel, D. Haskel, E. A. Stern, and Y. Yacoby, Physica B **208**, **209** (1995), 154.
[13] X. Yang and P. W. Blosser, Zeolites **17** (1996), 237.
[14] Y. K. Krisnandi, R. F. Howe, and P. D. Southon, to be published.
[15] S. Kuznicki, U.S. Patent 5, 011, 591 (1991).
[16] Y. Su, M. L. Balmer, and B. C. Bunker, J. Phys. Chem. **104** (2000), 8160.
[17] P. D. Southon and R. F. Howe, Chem. Matter. **14** (2002), 4209.
[18] Y. Krisnandi, M.Sc. Thesis: A Photoreactivity Study of Microporous Titanosilicate, University of New South Wales, Sydney, 2001.
[19] G. Sankar, R. G. Bell, J. M. Thomas, M. W. Anderson, P. A. Wright, and J. Rocha, J. Phys. Chem. **100** (1996), 3713.
[20] X. Yang and R. E. Truitt, J. Phys. Chem. **100** (1996), 3713.
[21] R. F. Howe and M. Gratzel, J. Phys. Chem. **89** (1985), 4495.

[22] R. D. Iyengar, Adv. Colloid. Interface Sci. **3** (1972), 365.
[23] R. Bal, K. Chaudhari, D. Srinivas, S. Sivisankar, and P. Ratnasamy, J. Mol. Catal. A **162** (2000), 199.
[24] M. Che and A. J. Tench, Advances in Catal. **32** (1983), 2.
[25] L. J. Bellamy, The Infrared Spectra of Complex Molecules, 3rd Edition, Chapman and Hall, London, 1975.
[26] G. Herzberg, Molecular Spectra and Molecular Structure, II Infrared and Raman Spectra of Polyatomic Molecules, Van Nostrand, Princeton, 1959.
[27] A. Zecchina, F. X. L. I. Xamena, *et al.*, Phys. Chem. Chem. Phys. **3** (2001), 1228
[28] M. Che and A. J. Tench, Advances in Catal. **31** (1982), 77.
[29] C. O. Arean, G. T. Palomino, A. Zecchina, S. Bordiga, F. X. L. I. Xamena, and C. Paze, Catalysis Lett. **66** (2000), 231.
[30] D. Park, J. Zhang, K. Ikeue, H. Yamashita, and M. Anpo, J. Catalysis Letters **185** (1999), 114.
[31] S. Yamazaki, S. Tanaka, and H. Tsukamoto, J. Photochem. & Photobiol. A: Chem. **121** (1999), 55.
[32] X. Fu, A. C. Louis, W. A. Zeltner, and M. A. Anderson, J. Photochem. Photobiol. A: Chem. **97** (1996), 181.